Development of an auxiliary propulsion module for an autonomous underwater glider

Claus, B.; Bachmayer, R.; Williams, C. D.

Publisher's version / Version de l'éditeur:
https://doi.org/10.1243/14750902JEME204
Journal of Engineering for the Maritime Environment, 224, 4, pp. 255-266, 2010-06-03

Development of an auxiliary propulsion module for an autonomous underwater glider

B Claus[1], **R Bachmayer**[1*], and **C D Williams**[2]
[1]Faculty of Engineering and Applied Science, Memorial University of Newfoundland, St. John's, Newfoundland and Labrador, Canada
[2]Institute for Ocean Technology, National Research Council Canada, St. John's, Newfoundland and Labrador, Canada

The manuscript was received on 17 January 2010 and was accepted after revision for publication on 3 June 2010.

DOI: 10.1243/14750902JEME204

Abstract: A low-power propeller-based propulsion module has been developed to augment the buoyancy engine of a 200 m Slocum electric glider. This device is introduced to allow new behaviours such as horizontal flight and faster overall speeds to expand the existing operational envelope of underwater gliders. The design of the system is optimized for use at the typical horizontal glider speed of 0.3 m/s. Before integration into the glider the stand-alone propulsion module has been tested in a small flume tank to verify the systems performance. The validity of a previously published hydrodynamic model of the glider at zero angle of attack was verified by conducting drag measurements at various flow velocities at full scale in a larger flume tank. Self-propulsion tests were also performed to establish the performance of the glider with the new propulsion module in the larger flume tank and in the university tow tank. The results from these tests show that the new propulsion module is able to match the performance of the conventional glider for full depth profiles and to exceed it for limited depth profiles.

Keywords: auxiliary propulsion module, autonomous underwater glider, hydrodynamic model, self-propulsion tests

1 INTRODUCTION

Over the past 10 years, autonomous underwater gliders have become increasingly useful for oceanographic research [**1**]. Gliders use an active buoyancy control system combined with a set of fixed wings to move vertically and horizontally in a sawtooth-like pattern through the water column [**2**–**4**]. The endurance of these underwater vehicles varies from weeks to several months and even longer in the case of the thermal glider [**4**]. In contrast, currently available propeller-driven autonomous underwater vehicles (AUVs) achieve endurances ranging from hours to days. This stark contrast can mostly be attributed to a purpose-built system and to the low speed at which the gliders move [**5**, **6**]. Gliders typically move at horizontal speeds of about 0.3 m/s compared with propeller-driven AUVs which typically move at average speeds greater than 1.0 m/s. The low-speed capability can create significant problems when operating in areas of strong water currents which exceed the glider's maximum forward speed. If the direction of the currents is known *a priori* or measured *in situ* [**7**], the missions can be designed either to avoid these areas or to take advantage of them. In this case the operator must redirect the glider to deal with the current better by moving away from that region or, in the case of significant vertical stratification, to try to operate below or above the expected layer of highest lateral velocities. However, unknown currents can pose a significant risk to the successful execution of the mission plan. These issues have given rise to the idea of the hybrid glider which combines the gliding behaviours of traditional underwater gliders with the propeller-driven behaviours of AUVs. Two additional hybrid AUV–glider platforms are being developed and have been reported in references [**8**] and [**9**].

In this paper the design and testing of an auxiliary propulsion module for the Slocum class of underwater

*Corresponding author: Faculty of Engineering and Applied Science, Memorial University of Newfoundland, Prince Philip Drive, St. John's, Newfoundland and Labrador A1B 3X5, Canada. email: bachmayer@mun.ca

gliders are addressed. The objectives of the project are to enable the glider to move horizontally at the nominal glider speed of 0.3 m/s and, for short periods of time, to double its horizontal speed to approximately 0.6 m/s. To this end a simplified mathematical model of underwater gliders as well as a model for the Slocum 200 m glider ballast pump power consumption based on experimental data are described. These two models are used to develop design constraints and initial design component selection. The design and the testing process for the propeller and motor are presented in which the final configuration is shown. Following this, the mechanical, electrical, and software integration of the module into the existing glider is discussed. Section 5 describes results from system testing and evaluation including experimental results from full-scale tests at the Marine Institute (MI) of Memorial University of Newfoundland (MUN) and tow tank self-propulsion tests at the Ocean Engineering Research Centre at MUN. The last section summarizes the results of the design and evaluation phase of the hybrid glider and gives an overview of the next steps in the development of the hybrid glider towards a fully operational system.

2 GLIDER MODEL

2.1 Hydrodynamic model

For the purpose of the propulsion system design the glider shown in Fig. 1 was assumed to be ballasted neutrally buoyant, and trimmed for level flight at a pitch angle $\theta = 0^\circ$. Furthermore, the glider is assumed to be moving at a constant speed. These assumptions are not valid for regular glider operations but for the initial design purpose they provide a valid starting point while simplifying the lateral plane hydrodynamic model of gliders as presented in reference [**10**]. As a result the glide-path angle $\xi = 0^\circ$ and therefore the angle of attack $\alpha = 0^\circ$ as well.

The standard model for hydrodynamic lift F_L and drag F_D can be written

$$F_L = \frac{1}{2}\rho A C_L(\alpha) V_A^2 \tag{1}$$

$$F_D = \frac{1}{2}\rho A C_D(\alpha) V_A^2 \tag{2}$$

where ρ is the fluid density, A is the cross-sectional area, and V_A is the advance velocity. Graver *et al.* [**11**] presented a hydrodynamic model and identified the model parameters for a Slocum 200 m underwater glider.

From equation (1) the lift coefficient $C_L(\alpha)$ based on the frontal area was determined as

$$C_L(\alpha) = 11.76\alpha + 4.6\alpha|\alpha| \tag{3}$$

and from equation (2) the drag coefficient $C_D(\alpha)$ based on frontal area as

$$C_D(\alpha) = 0.214 + 32.3\alpha^2 \tag{4}$$

Under the assumption $\alpha = 0^\circ$ the model simplifies to a drag-only model as expected for a symmetric body, with $C_D(\alpha = 0) = C_{D_0} = 0.214$ such that

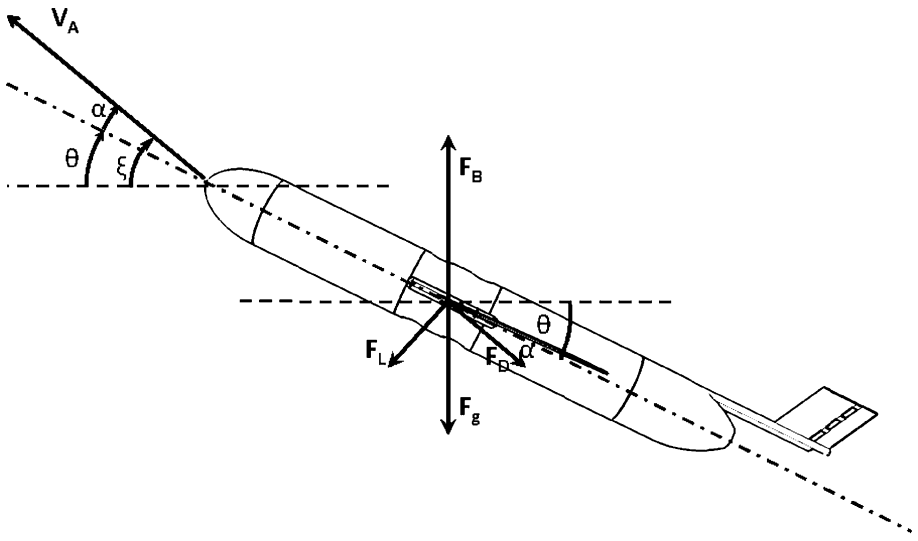

Fig. 1 Schematic diagram of an autonomous underwater glider defining the body forces, velocities, and angles

$$F_{\mathrm{D}} = \frac{1}{2}\rho A C_{\mathrm{D}_0} V_{\mathrm{A}}^2 \tag{5}$$

Under the assumption of constant velocity, there is no acceleration; therefore added mass effects can be neglected and the equation of motion is reduced to the balance of the drag force F_{D} and the thrust generated by the propulsor.

2.2 Ballast pump power consumption

To establish the power usage of a buoyancy-driven glider the power to the ballast pump was monitored during a mission with various depths of profiles where one profile is a complete up-and-down cycle. The ballast pump turns on only at the inflection points of a profile, at either the highest or the lowest points of the cycle. From these measurements the instantaneous power for a given depth may be plotted as in Fig. 2, establishing the load line for the pump as a function of depth as

$$P_{\mathrm{bpi}} = 0.3z + 8.2 \tag{6}$$

where z is the glider depth, the coefficient 0.3 has the units watts per metre, and 8.2 W is the ballast pump power at the surface. The time-averaged power P_{bp} is then given by converting the instantaneous power to the energy E_{bp} consumed per profile with one use of the buoyancy pump at the surface and one at depth and dividing by the total cycle time t_{bp} according to

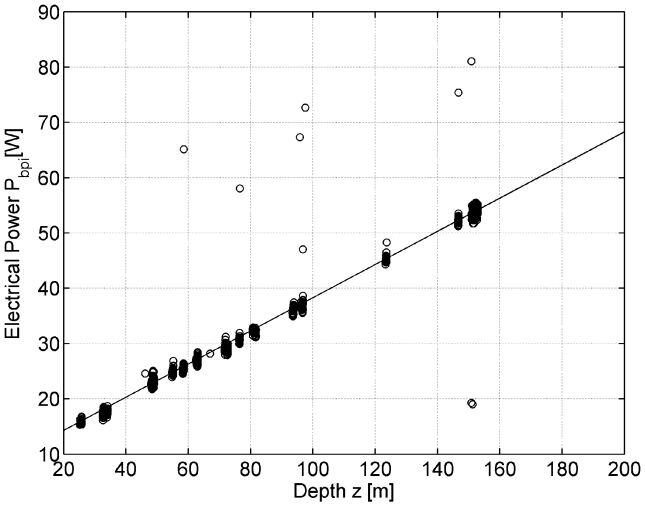

Fig. 2 Ballast pump instantaneous power at depth with outliers due to motor current transients during start-up. The trend line shows a linear fit through the data

$$E_{\mathrm{bp}} = (0.3z + 8.2)30 + 164 \tag{7}$$

$$P_{\mathrm{bp}} = \frac{E_{\mathrm{bp}}}{t_{\mathrm{bp}}} \tag{8}$$

Here the shallow inflection depth is assumed always to be at the surface $z = 0$ and the time that the pump is on at the surface is 20 s, resulting in an energy of 164 J. At depth the pump is on for 30 s.

3 PROPULSION MODULE DESIGN

3.1 Design constraints

To minimize the impact of the propulsion unit on the original performance of the glider, certain constraints were placed on the design. The module should be able to be turned on and off to allow the glider to retain its normal buoyancy-driven method of operation. In light of this, during regular operations, the influence of the propulsion unit on the hydrodynamic performance of the glider should be minimized. The impact of the propulsion module on the glider's endurance and range when propelled for horizontal flight at typical glide speeds should be such that the propulsor should consume equal power to or less power than the buoyancy engine. Also, the module should be capable of providing sufficient thrust to enable a sprint mode at least to double the glider's typical speed for short durations. These constraints provide a unique challenge in developing a high-efficiency low-power propulsion module.

3.2 Design

To design a prototype device within these constraints an overall concept was chosen which utilized an electric motor, magnetic coupling, and folding propeller. These components require careful design matching to ensure that the peak operational regions overlap one another. To this end, electric motors provide the necessary energy density for a small low-power device and provide good efficiency-matching potential to peak propeller efficiencies. A magnetic coupling was selected to minimize frictional losses due to shaft seals.

Initial matching of the motor, gearbox, and propeller was achieved by using the simplified drag force model and nominal glider operational parameters as a reference for design. The energy flow for the system is shown in Fig. 3, where the product of

the inputs over the product of the outputs is equal to the efficiency of the particular subsystem. The system efficiency η_{sys} is then given as the product of the subsystem efficiencies according to

$$\eta_{sys} = \eta_m \eta_{gb} \eta_{mc} \eta_p \tag{9}$$

where η_m is the motor efficiency, η_{gb} is the gearbox efficiency, η_{mc} is the magnetic coupling efficiency, and η_p is the propeller efficiency. The efficiency of the motor controller may be included in η_{sys} as well. However, for this design a high-quality brushed motor with precious- metal brushes was chosen with the final design to be driven directly from the rail voltages of 3.3 V and 14.4 V to give a high-speed operation point and a low-speed operation point respectively. The motor controller efficiency was therefore omitted from the system efficiency definition. Also omitted from the system efficiency definition is the battery performance, which is the product of environmental conditions and the electrical load requirements. The effects of the environmental conditions are omitted because they apply to buoyancy-driven vehicles and propeller-driven vehicles alike. The electrical load for the auxiliary propulsion module is a small continuous load while the load for the buoyancy engine is large and highly intermittent. This difference can have an impact on the battery performance owing to I^2R losses. The I^2R losses due to the auxiliary propulsion module operation are O(0.001 W) and for the buoyancy engine operation they are O(0.01 W), where R, in this case, is the internal resistance of the batteries equal to 0.136 Ω [**12**].

In general, the motor efficiency may be given as [**13**]

$$\eta_m = \frac{\tau_m \Omega_m}{iv} \frac{2\pi}{60} \tag{10}$$

where the motor torque τ_m is given by

$$\tau_m = k_1 (i - i_0) \tag{11}$$

and the motor speed Ω_m is given by

$$\Omega_m = vk_2 - k_3 k_1 (i - i_0) \tag{12}$$

The resulting motor efficiency depends on only the input voltage v and current i according to

$$\eta_m = \frac{k_1 (i - i_0)[vk_2 - k_3 k_1 (i - i_0)]}{iv} \frac{2\pi}{60} \tag{13}$$

where k_1, k_2, and k_3 are motor constants and i_0 is the motor no-load current. The propeller was modelled as a small-blade-area-ratio propeller using the OpenPVL MATLAB® scripting [**14**]. The gearbox was assigned a fixed efficiency due to mechanical losses as given by the data sheet from the manufacturer. The magnetic coupling efficiency was assumed to be constant irrespective of motor or propeller selection and was therefore removed from the parameter space for the purposes of propeller, motor, and gearbox matching.

The output of this model was plotted for different motor, propeller, and gearbox combinations to match the peak efficiencies, as in Fig. 4, for a given shaft speed and propeller inflow velocity. The peak efficiencies for electric motors generally occur for speeds that are higher than the peak efficiency for propellers. Gearboxes are therefore used to match the speed of a given motor to the peak operational region of the propeller. However, for each stage of gear reduction, additional mechanical losses are accrued by the gearbox, thus reducing its efficiency. These parameters compete against one another and, by iterating the gearbox, motor, and propeller parameters, a motor and gearbox combination showing peak performance for the theoretical small-blade-area-ratio propeller and nominal glider operational conditions may be chosen. The gearbox used for this design is a dual-stage planetary gearbox with $\eta_{gb} = 81$ per cent.

Since the level of input energy is very low, O(1 W), all stages of energy conversion were considered and all losses were minimized. Shaft seal frictional losses, which in a more powerful system account for only a

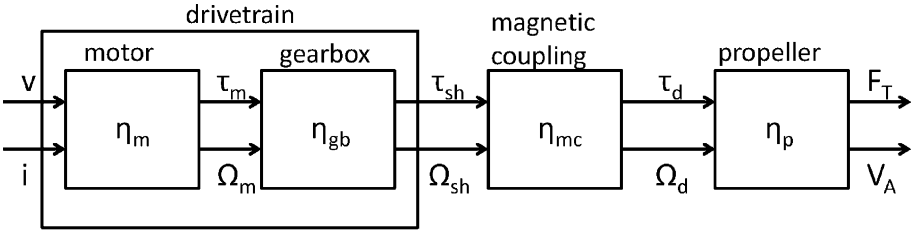

Fig. 3 Energy flow diagram showing the inputs and outputs for each stage of energy conversion

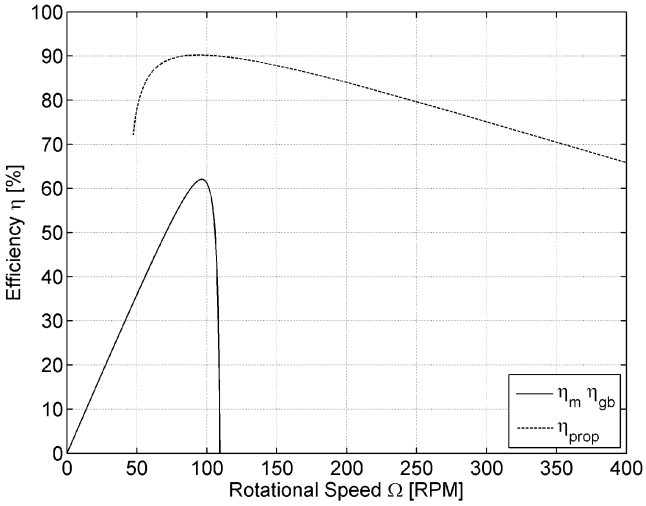

Fig. 4 Example motor and propeller efficiency plot showing the matching peak efficiencies

fraction of the total power, dominate in low-power systems. To this end, a magnetic coupling was used and designed such that the pull-out torque was just beyond the theoretical requirements required for the propeller to move the glider at a sprint speed of 0.75 m/s. However, magnetic couplings often require additional bearings, and the lubrication and seals on bearings consume a large portion of the power of a 1 W system. Therefore, ultra-low-friction dry-lubricated ceramic bearings were used to reduce these losses. The losses from the magnetic coupling and bearings were quantified through analysis of the motor input current before and after assembly. For the maximum voltage condition, this difference equates to a change in current of 3 mA, resulting in less than 0.001 N m frictional torque in the magnetic coupling assembly, which is 10 per cent of the no-load torque and 1 per cent of the full-load torque.

3.3 Propeller selection and testing

Since the thrust requirements of the system are relatively low, the ideal actuator disc efficiency is high, as shown by [**15**]

$$\eta_{\mathrm{I}} = \frac{2}{1+\sqrt{2F_{\mathrm{T}}/\left(\rho A V_{\mathrm{A}}^2\right)+1}} \tag{14}$$

where F_{T} is the thrust. However, no suitable folding underwater propellers were found with published torque and thrust data. Therefore, a series of folding propellers was tested to determine their operating parameters experimentally. Propellers with various diameters and pitch ratios were selected for tests, as shown in Fig. 5.

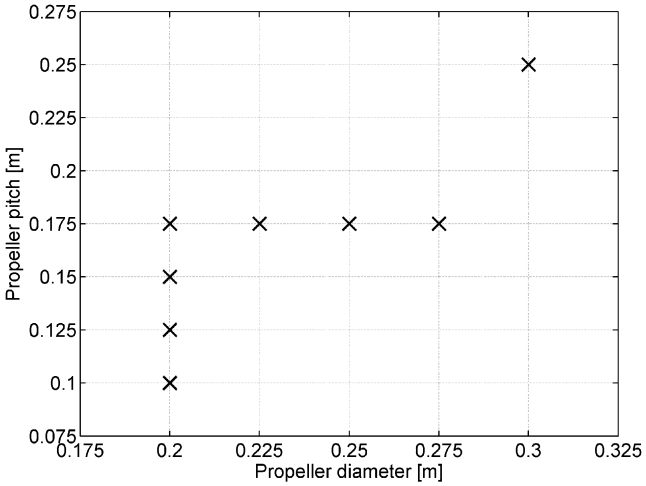

Fig. 5 Selection of propellers for tests in the MUN flume tank

To characterize these propellers, V_{A}, F_{T}, v, and i were measured using the experimental set-up shown in Fig. 6, utilizing the 0.3 m × 0.5 m × 5 m flume tank at MUN. The electrical current and voltage were measured using a Hall-effect current sensor and a resistive voltage divider. The thrust was measured using a lever to amplify the force and an Omega LCAE 6 kgf load cell with a Dataforth DSCA38-05 signal conditioner. The thrust measurement F_{T} is computed from the measured value as

$$F_{\mathrm{T}} = 1.8715(F_{\mathrm{M}} - F_0) \tag{15}$$

where 1.8715 is the lever ratio, F_0 is the drag force on the measurement apparatus, and F_{M} is the measured force. These values were read into MATLAB® for further processing using the Data Acquisition Toolbox and a National Instruments® USB-6211 data acquisition system. The advance velocity V_{A} of the water was measured using a SonTek ADVOcean

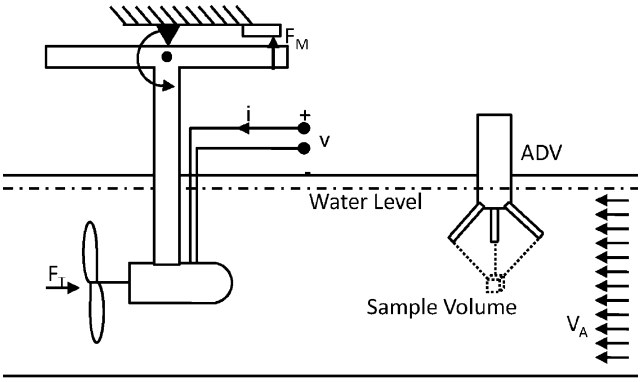

Fig. 6 Schematic diagram of the MUN flume tank test for propulsion system characterization (ADV, acoustic Doppler velocimeter)

acoustic Doppler velocimeter. Tests were performed for flow speeds of 0.3 m/s, 0.4 m/s, and 0.5 m/s where the input current to the motor was controlled from 0 A to the pull-out torque at 0.3 A. The measured system efficiency η_{sysm} may therefore be calculated as

$$\eta_{\text{sysm}} = \frac{F_{\text{T}} V_{\text{A}}}{iv} \tag{16}$$

Using the motor model presented in equation (13), the propeller and motor efficiencies may be deduced from the system efficiency according to

$$\eta_{\text{p}} = \frac{F_{\text{T}} V_{\text{A}}}{\tau_{\text{m}} \Omega_{\text{m}}} \frac{60}{2\pi} \tag{17}$$

and in equation (9) where τ_{m} and Ω_{m} are as in equations (11) and (12) respectively. It should be noted that the mechanical losses in the magnetic coupling and bearings will be lumped in with the propeller efficiency. Samples of the results of these tests are shown in Fig. 7.

By analysing the peak efficiencies from these data, an optimum propeller of 0.225 m diameter and 0.175 m pitch may be selected for use on the hybrid glider. However, the selection above does not take into account the interaction between the propeller and the hull of the glider. The wake fraction w and thrust deduction factor t affect the performance of the propeller through the hull efficiency η_{h} as shown by [**16**]

$$\eta_{\text{d}} = \eta_{\text{sys}} \eta_{\text{h}} = \eta_{\text{sys}} \frac{1-t}{1-w} \tag{18}$$

Estimates of the wake fraction from a computational fluid dynamics (CFD) model give values of $w = 0.34$ and $w = 0.296$ for propellers of 0.2 m and 0.225 m diameters respectively for $V_{\text{A}} = 0.5$ m/s. These values, combined with an assumed thrust deduction factor $t = 0.2$ from reference [**16**], result in $\eta_{\text{h}} = 1.212$ for the smaller propeller and $\eta_{\text{h}} = 1.136$ for the larger propeller, as shown in Fig. 8. However, the relative difference in the open-water system efficiency from the MUN flume tank tests for these two propellers is only 2 per cent. Additionally, the torque requirements of the 0.175 m pitch propeller were such that the magnetic coupling stalled at full power. For these reasons, a propeller with 0.2 m diameter and 0.15 m pitch was selected for the propulsion module.

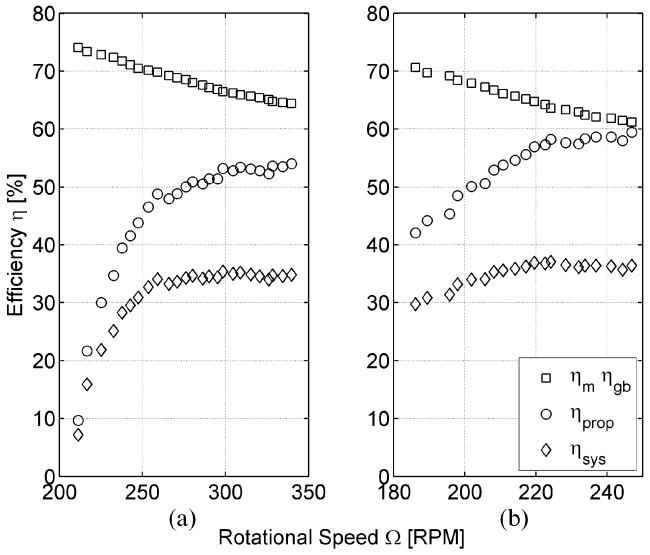

Fig. 7 MUN flume tank test results for (a) a 0.2 m propeller diameter with a 0.15 m propeller pitch and (b) a 0.225 m propeller diameter with a 0.175 m propeller pitch for an advance velocity of 0.5 m/s

4 SYSTEM INTEGRATION

The integration of the propulsion module into the glider was carried out in such a way that minimal changes would be necessary. Mechanically, the propulsion module was designed so that it replaces the 0.5 kgf emergency drop weight at the rear of the glider. To this effect, the weight in water of the propulsion module is matched to the weight in water of the drop weight. This location has the added benefit of being directly in line with the centre of buoyancy of the vehicle; however, it currently removes the function of the emergency drop weight. Future versions are to integrate the function of the

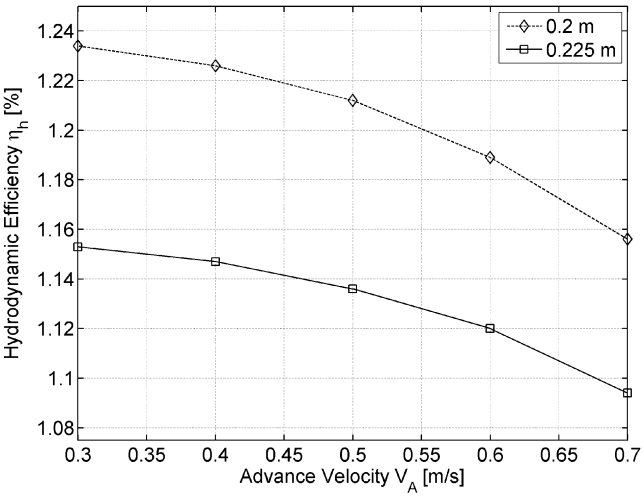

Fig. 8 Hull efficiency from the CFD model for 0.2 m and 0.225 m diameter propellers

drop weight with the propulsion module so that it is ejected in emergencies.

Electrically, the glider has two computers connected by a communications bus. The glider computer handles all control and low-level functions while the science computer is used for integration of new payloads and sensors. To avoid changing the existing glider architecture the propulsion module is connected to the power pins on the science computer board used for powering payload instruments. For testing purposes the motor is controlled through a full bridge motor controller and the power is monitored through a resistive voltage divider and Hall-effect current sensor. However, in future versions the motor will be run off the rail supply voltages in the glider to remove the electrical losses associated with the motor controller.

In software, the on–off and duty cycle control is managed through a custom interface application written for the science computer operating system. This application queries the glider computer for the control variables and then sends commands to the motor controller and power monitor devices. It also retrieves the data from the power-monitoring sensors and logs the data in the science computer's memory. Additionally, the time stamp for the data recorded is exchanged with the glider computer to allow post synchronization of the data sets.

5 SYSTEM EVALUATION AND TESTING

5.1 Flume tank drag and propulsion tests

Full-scale drag and propulsion tests were performed at the MI's flume tank with a test section 8 m × 4 m × 22.5 m and capable of generating flow speeds from 0 m/s to 1 m/s. These tests were made to verify the glider's hydrodynamic model and to evaluate its propulsion abilities. The general experimental set-up is shown in Fig. 9 with an expanded view of the attachments to the glider in Fig. 10. In this set-up the glider is attached to a guide wire which constrains the glider in yaw, pitch, and roll. Drag measurements were then performed through a load cell attached to the forward end of the glider. Additional drag and self-propulsion experiments were performed with another load cell attached to the aft end of the glider and pre-tensioned with a counterbalance weight. The forward attachment point was through the nose, and the aft attachment was through a twin-bridle harness attached well outboard on each wing in order to provide clearance for the propeller to spin freely.

The drag tests were performed for the glider at zero angle of attack with wings, without wings, and with wings and the counterbalance weight. Self-propulsion tests were performed for the glider with the counterbalance weight by varying the voltage to

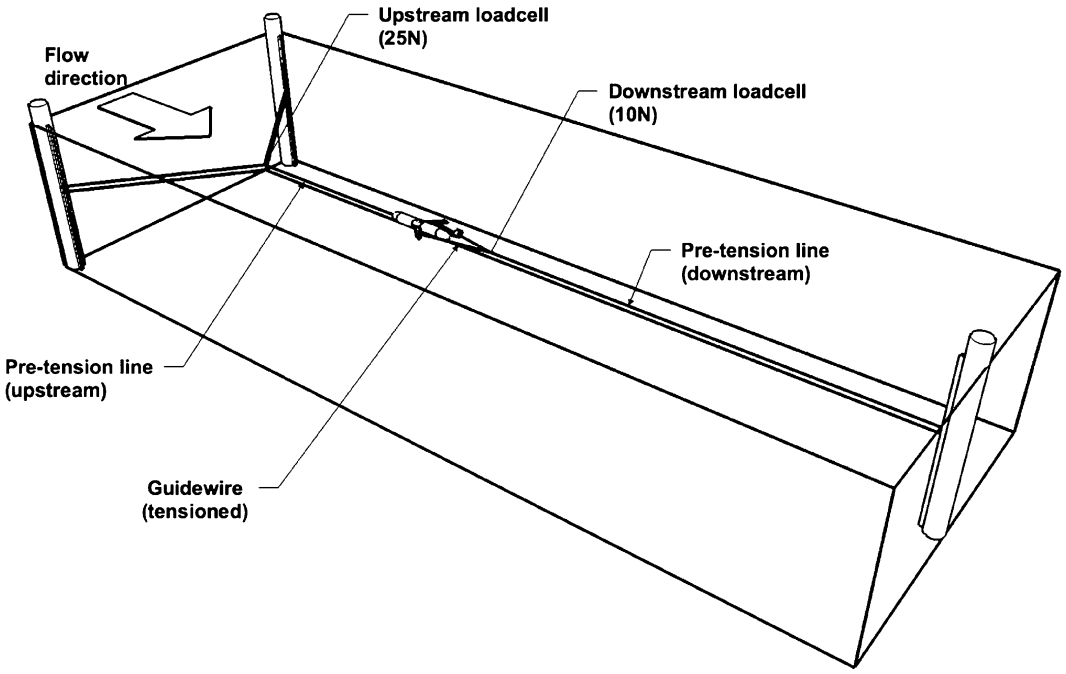

Fig. 9 MI 4 m × 8 m × 22 m flume tank experimental set-up for full-scale glider hydrodynamic and propulsion testing

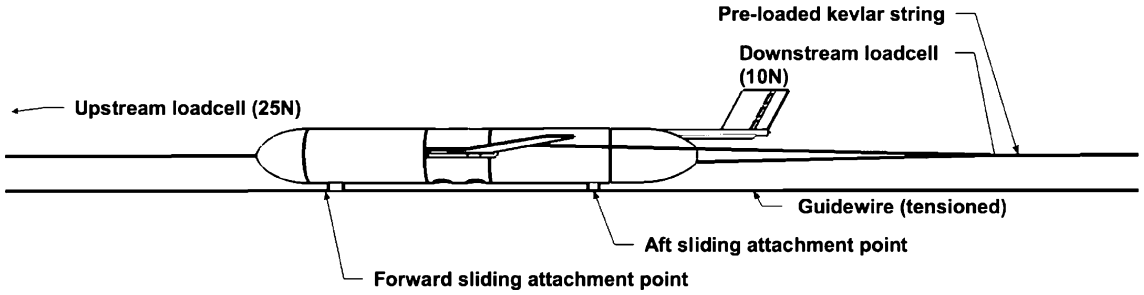

Fig. 10 Expanded view of the MI flume tank experimental set-up

the motor. These tests were performed for advance velocities from 0.2 m/s to 1.0 m/s in increments of 0.1 m/s. For all tests the motor voltage v and current i and also the glider drag force F_D were recorded. For the counterbalanced measurements, F_D was calculated by subtracting the aft load cell readings from the forward load cell reading to remove the effect of the preloading. The MI's flume tank had been previously calibrated such that the advance velocity was recorded from the commanded set point and not actively measured. The effects of the harness attached to the wings for the counterbalance were quantified through the difference between the drag test with and without the counterbalance. The results of the drag forces exerted on the glider for the different tests are shown in Fig. 11 with the self-propulsion test results shown in Fig. 12.

When compared with the drag for zero angle of attack in equation (4) the measured drag is found to be higher. At a speed of 0.3 m/s the measured drag force was 0.5 N and the predicted drag force was 0.34 N, a difference of nearly 50 per cent. This difference can partially be attributed to parasitic drag in the test set-up; however, the drag presented in equation (4) is based on indirect measurements and extrapolated to the zero-angle-of-attack condition. Therefore, the measurements presented here are considered to be more accurate for this case. The amount of electrical power required for horizontal flight using the auxiliary propulsion module is shown to be

$$P_{\text{prop}} = 13.2V_A^3 - V_A^2 + 1.1V_A \tag{19}$$

using a polynomial cubic fit to the MI flume tank power data in Fig. 12. Where the coefficient 13.2 has the units kilograms per metre, the coefficient -1 has the units kilograms per second and the coefficient 1.1 has the units kilogram metres per second. From equation (5) a cubic relationship is expected for hydrodynamic power which is different from the cubic polynomial in equation (19). A cubic polynomial was used as the correlation to the data was much stronger. The present authors attributed this difference to the non-simple body form of the

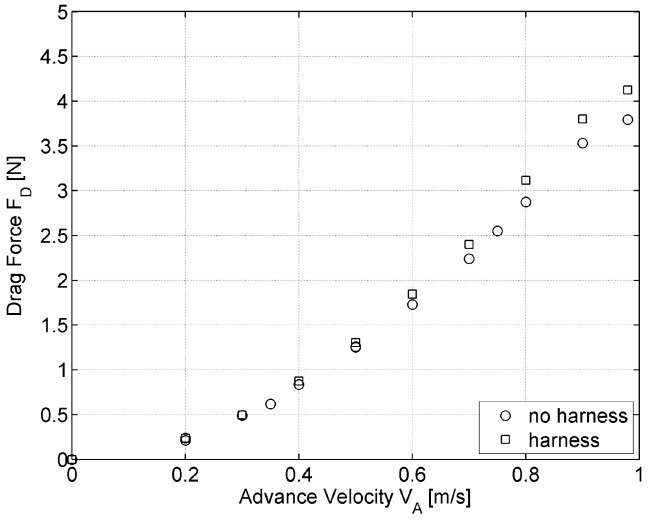

Fig. 11 MI flume tank glider hydrodynamic drag force measurement calibration and testing

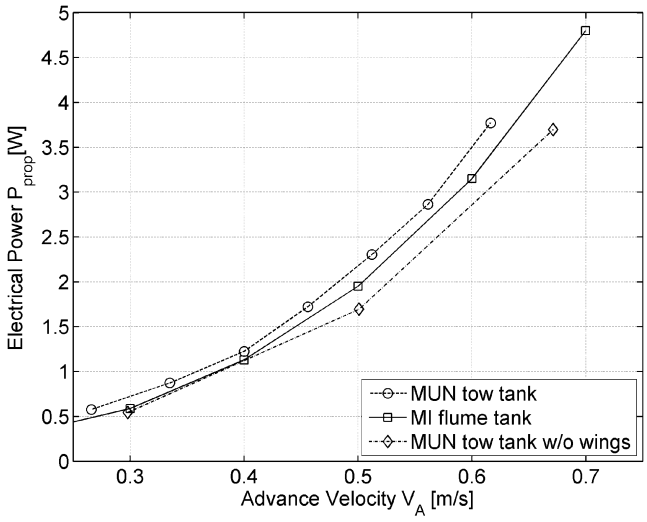

Fig. 12 Self-propulsion test results, comparing the MI flume tank experiments with the MUN tow tank experiments

vehicle and various advance velocities which resulted in flow transitions around the sensors, wings, and other body protrusions.

5.2 Tow tank self-propulsion experiments

Self-propulsion tests were performed in the tow tank at MUN to evaluate further the glider's propulsive capabilities. The experimental set-up for these tests was similar to that for the MI tests. However, for these tests the glider was attached only to a guide wire and not attached to the load cells, allowing the glider to move under self-propulsion while being constrained directionally.

The propulsion tests were performed for the glider with and without wings. In each case the voltage to the motor was varied and the glider's velocity and input electrical power were measured. The results from these tests are shown in Fig. 12 as well. The tow tank self-propulsion tests include friction effects due to the movement of the glider and its attachment to the guide wire. Additionally, the amount of ballast to tension the guide wire to make it ideally level was impractical for the length of the tank and therefore $\theta \neq 0^\circ$. The MI flume propulsive power requirements were lower than the MUN tow tank power requirements. This difference is attributed to the friction of the guide wire and $\theta \neq 0^\circ$ for the tow tank self-propulsion tests and therefore the MI flume tank self-propulsion results are considered to be the more accurate.

5.3 Range estimates

The range of an underwater vehicle is a function of the energy available, the power consumed, and the advance velocity [**17**]. This may be extended to buoyancy-driven gliders where the range R_{bp} becomes

$$R_{\text{bp}} = \frac{EV_{\text{bp}}}{P_{\text{bp}} + P_{\text{h}} + P_{\text{l}}} \tag{20}$$

where the ballast pump load P_{bp} is the propulsive load from equation (8), the available energy $E = 8\,\text{MJ}$, the hotel power $P_{\text{h}} = 0.2\,\text{W}$, and the sensor load $P_{\text{l}} = 1\,\text{W}$ [**1**]. The glider horizontal velocity V_{bp} is based on the glide path angle ξ and depth rate $\dot{z}$ as in

$$V_{\text{bp}} = \frac{\dot{z}}{\tan(\xi)} \tag{21}$$

where $\dot{z}$ is taken from reference [**18**] as

$$\dot{z} = 0.01333\xi - 0.125 \tag{22}$$

The range of values for ξ has been taken from field data as $29^\circ < \xi < 35^\circ$ for $20^\circ < \theta < 30^\circ$ and extrapolated to $15^\circ < \xi < 35^\circ$ to show the full range of velocities for the glider [**19**].

For a propeller-driven vehicle the range R_{prop} becomes

$$R_{\text{prop}} = \frac{EV_{\text{prop}}}{P_{\text{prop}} + P_{\text{h}} + P_{\text{l}}} \tag{23}$$

where the propulsion module load P_{prop} is defined as in equation (19). The propulsive velocity V_{prop} varies from 0.2 m/s to 0.67 m/s, the maximum speed from the MUN tow tank self-propulsion results.

For a glider operating with a bathtub-shaped trajectory, the buoyancy engine brings the glider to depth and the propeller is used at that point to move the glider horizontally by a distance d_{prop} until it is time for the next surfacing, at which point the buoyancy is increased to bring the glider back to the surface. In this case the range R_{hybrid} is

$$R_{\text{hybrid}} = \frac{E\left(V_{\text{bp}}\Delta_{\text{bp}} + V_{\text{prop}}\Delta_{\text{prop}}\right)}{P_{\text{bp}}\Delta_{\text{bp}} + P_{\text{prop}}\Delta_{\text{prop}} + P_{\text{h}} + P_{\text{l}}} \tag{24}$$

where Δ_{bp} and Δ_{prop} represent the ratio of time for which each propulsion method is active to the total time according to

$$\Delta_{\text{bp}} = \frac{t_{\text{bp}}}{t_{\text{bp}} + t_{\text{prop}}} \tag{25}$$

and

$$\Delta_{\text{prop}} = \frac{t_{\text{prop}}}{t_{\text{bp}} + t_{\text{prop}}} \tag{26}$$

The time t_{prop} that the propeller propulsion is active and the time t_{bp} that the buoyancy pump propulsion is active are defined as

$$t_{\text{prop}} = \frac{d_{\text{prop}}}{V_{\text{prop}}} \tag{27}$$

and

$$t_{\text{bp}} = \frac{2z}{\dot{z}} \tag{28}$$

respectively, where the horizontal distance travelled is $d_{\text{prop}} = 2500\,\text{m}$.

If R_{bp}, R_{prop}, and R_{hybrid} are plotted as functions of V_{bp}, V_{prop}, and V_{hybrid}, it can be seen that the buoyancy-driven glider and the hybrid glider exhibit similar range capabilities as shown in Fig. 13(a) when the glide depth $z = 200$ m. However, the hybrid glider is capable of travelling at faster overall speeds and has a significantly larger range than a conventional glider with asmall glide depth $z = 10$ m, as shown in Fig. 13(b). It should also be noted that in Fig. 13 the horizontal distance d_{prop} travelled while at depth z is set to 2500 m. If d_{prop} is decreased, the vehicle spends more time gliding to depth relative to moving horizontally at depth, causing R_{hybrid} and the time-averaged horizontal velocities to decrease towards the R_{bp} curve. To illustrate this behaviour, two cases may be examined at the extreme ends: the cases of the vehicle with $t_{bp} = 0$ s and of the vehicle with $t_{prop} = 0$ s. With $t_{bp} = 0$ s, the vehicle stays at the surface and the buoyancy engine is not used at all. The range for this case is given by R_{prop}. When $t_{prop} = 0$ s, the propeller is not used at all and the vehicle behaves as an unmodified glider. The range for this case is given by R_{bp}. This model does not take into account the settling times for the vehicle changing between operational modes or at the top or bottom of the inflection of the glide path. Additionally, the time spent on the surface is neglected. These omissions become increasingly important for gliding vehicles with shallow inflections as transitions occur with greater frequency.

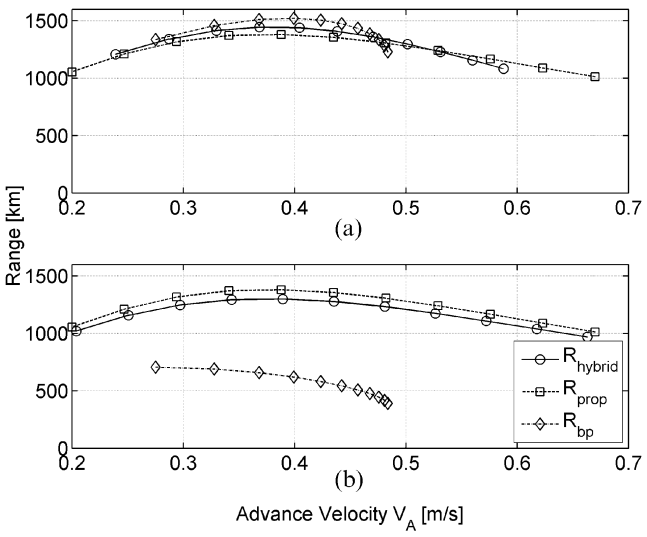

Fig. 13 Estimated range for a glider operating in hybrid mode, propeller-only mode, and ballast-pump-only modes with (a) full 200 m depth dives and (b) 10 m average depth dives

6 CONCLUSIONS AND FUTURE WORK

An auxiliary propulsion module for a 200 m Slocum glider has been presented. The module greatly enhances the operational abilities of underwater gliders by enabling horizontal flight and increased speed capabilities. A simplified hydrodynamic model under the assumption of a zero angle of attack was used to design the module. Using this model, the initial component selection was accomplished through matching the motor, gearbox, and measured propeller efficiencies. The propulsion module's performance was confirmed through propulsion tests in the flume tank at MUN. Upon integration of the propulsion module into the glider, self-propulsion tests were conducted in the $4\,\text{m} \times 8\,\text{m} \times 22\,\text{m}$ flume tank at the MI. Direct measurements of the drag force for the glider at zero angle of attack were also performed in the MI flume tank in order to verify the simplified hydrodynamic model; the measured drag force was found to be 0.5 N for an advance velocity of 0.3 m/s, nearly 50 per cent higher than the predicted value of 0.34 N at 0.3 m/s. Additional, directionally constrained self-propulsion tests were executed in the MUN tow tank 53 m long to verify the performance of the hybrid glider. The self-propulsion tests show that the propulsion module is capable of moving the glider horizontally at 0.3 m/s while consuming 0.6 W of battery power and at 0.67 m/s using 4.25 W. A comparison of the power requirements for the propulsion of conventional gliders with the power consumed by this auxiliary propulsion module shows that the power consumed is about the same for full-depth glides to 200 m. When used only for shallow-water operations, the time-averaged power consumed by this module is less than that consumed by the conventional glider. This performance results in the potential for equal ranges for hybrid and conventional modes of operation when used appropriately; additionally, the auxiliary propulsion module enables new modes of operation such as movement in the lateral plane and higher overall velocities.

The hybrid glider's expansion of abilities opens up many new roles and opportunities for collaborations using underwater gliders. The auxiliary propulsion module is capable of operating at depths over 1000 m, allowing it to be transferred to 1000 m gliders as well. The 1000 m variant of the Slocum glider would require only some wiring and software additions to integrate it into its systems. Potential future collaborations will involve investigating the propulsive performance of the auxiliary propulsion versus the deep glider as the ballast system on the deep gliders uses a pump rather than a piston to maintain efficiency in deep water.

During our full-scale trials in the tow tank as well as in the flume tank the glider's motions at various velocities have been observed. It was evident that at high speeds (velocities exceeding 0.5 m/s) the pitching motions of the glider became more pronounced, compared with the more benign motions at nominal glider speeds. This instability is not unexpected, and the next steps will include a careful stability analysis of the hybrid glider, using a dynamic model of the system, currently under development, as well as the integration of an accurate motion sensor for system identification purposes. Using the dynamic model a controller will be implemented to stabilize the undesired pitching motion during horizontal flight. Future work will also focus on developing the navigational algorithms and behaviours to govern extended autonomous missions using the propulsion module. Field trials of the hybrid glider system will be conducted during 2010.

ACKNOWLEDGEMENTS

The authors would like to thank Paul Winger, George Legge, and Tara Perry from the MI, Jack Foley and Craig Mitchell from MUN, Jeswin Jeyasuyra and Moqin He of the National Research Council Canada, Paul Lacroix and the Canadian Centre for Ocean Gliders for use of the glider and the Physical Oceanography Department at MUN for providing additional instrumentation and experimental support. This project is supported through funding provided by the Natural Sciences and Engineering Research Council, MUN, and Suncor-Petro Canada.

REFERENCES

1 **Rudnick, D. L., Davis, R. E., Eriksen, C. C., Fratantoni, D. M.,** and **Perry, M. J.** Underwater gliders for ocean research. *Mar. Technol. Soc. J.*, 2004, **38**, 73–84.

2 **Eriksen, C. C., Osse, T. J., Light, R. D., Wen, T., Lehman, T. W., Sabin, P. L., Ballard, J. W.,** and **Chiodi, A. M.** Seaglider: a long-range autonomous underwater vehicle for oceanographic research. *IEEE J. Oceanic Engng*, 2001, **26**(4), 424–436.

3 **Sherman, J., Davis, R. E., Owens, W. B.,** and **Valdes, J.** The autonomous underwater glider 'Spray'. *IEEE J. Oceanic Engng*, 2001, **26**(4), 437–446.

4 **Webb, D. C., Simonetti, P. J.,** and **Jones, C. P.** SLOCUM: an underwater glider propelled by environmental energy. *IEEE J. Oceanic Engng*, 2001, **26**(4), 447–452.

5 **Bradley, A. M.** Low power navigation and control for long range autonomous underwater vehicles. In Proceedings of the Second International Offshore and Polar Engineering Conference, San Francisco, California, USA, 14–19 June 1992, Vol. II, pp. 473–478 (International Society of Offshore and Polar Engineers, Golden, Colorado).

6 **Bradley, A. M., Feezor, M. D., Singh, H.,** and **Yates Sorrell, F.** Power systems for autonomous underwater vehicles. *IEEE J. Oceanic Engng*, 2001, **26**(4), 526–538.

7 **Merckelbach, L. M., Briggs, R. D., Smeed, D. A.,** and **Griffiths, G.** Current measurements from autonomous underwater gliders. In Proceedings of the Ninth IEEE/OES Working Conference on *Current Measurement Technology*, 2008, pp. 61–67 (IEEE, New York).

8 **Page, Y. L.** Innovative glider technologies. In Proceedings of the Third European Gliding Observatories Workshop and Glider School (*EGO 2008*), La Spezia, Italy, 27–31 October 2008.

9 **Caffaz, A., Caiti, A., Casalino, G.,** and **Turetta, A.** The hybrid glider/AUV Folaga. *IEEE Robotics Automn Mag.*, 2010, **17**(1), 31–44.

10 **Leonard, N. E.** and **Graver, J. G.** Model-based feedback control of autonomous underwater gliders. *IEEE J. Oceanic Engng*, 2001, **26**(4), 633–645.

11 **Graver, J. G., Bachmayer, R., Leonard, N. E.,** and **Fratantoni, D. M** Underwater glider model parameter identification. In Proceedings of the 13th International Symposium on *Unmanned Untethered Submersible Technology* (*UUST '03*), Durham, New Hampshire, USA, 24–27 August 2003.

12 Alkaline manganese dioxide battery MN1300, size D (LR20). Data Sheet, Duracell, Bethel, Connecticut, USA, June 2008.

13 Key information on – Maxon DC motor and Maxon EC motor, Maxon motor, Sachsein, Switzerland, 2005, available from http://test.maxonmotor.com/docsx/Download/catalog_2005/Pdf/05_034_e.pdf.

14 **D'Epagnier, K. P., Chung, H. L., Stairway, M. J.,** and **Kimball, R. W.** An open source parametric propeller design tool. In Proceedings of OCEANS 2007, 29 September–4 October 2007, pp. 1–8 (IEEE, New York).

15 **Lewis, E. V.** *Principles of naval architecture, resistance, propulsion, and vibration,* Vol. II, 2005 (Society of Naval Architects and Marine Engineers, Jersey City, New Jersey).

16 **Newman, J. N.** *Marine hydrodynamics*, 1977 (MIT Press, Cambridge, Massachusetts).

17 **Singh, H., Yoerger, D.,** and **Bradley, A.** Issues in AUV design and deployment for oceanographic research. In Proceedings of the. IEEE International Conference on *Robotics and Automation*, 1997, Vol. 3, pp. 1857–1862 (IEEE, New York).

18 **Graver, J. G.** *Underwater gliders: dynamics, control and design*, 2005 (Princeton University Press, Princeton, New Jersey).

19 **Williams, C. D., Bachmayer, R.,** and **deYoung, B.** Progress in predicting the performance of ocean

gliders from at-sea measurements. In: Proceedings of OCEANS 2008, 15–18 September 2008, pp. 1–8 (IEEE, New York).

APPENDIX

Notation

A	cross-sectional area (m^2)
C_D	drag coefficient based on the frontal area of the hull
C_{D_0}	drag coefficient for $\alpha = 0$ based on the frontal area of the hull
C_L	lift coefficient based on the frontal area of the hull
d_{prop}	horizontal distance for propeller-based travel (m)
E	battery energy (J)
F_D	drag force (N)
F_L	lift force (N)
F_M	measured thrust (N)
F_T	thrust (N)
F_0	test apparatus drag force (N)
i	motor input current (A)
i_0	motor no-load current (A)
k_1	torque constant (N m/A)
k_2	speed constant (r/min V)
k_3	motor constant (r/min N m)
P_{bp}	buoyancy-driven average propulsive power (W)
P_{bpi}	instantaneous ballast pump power (W)
P_h	hotel power (W)
P_l	load power (W)
P_{prop}	electrical input power to the propulsion module (W)
R_{bp}	conventional glider range (m)
R_{prop}	propeller-driven autonomous underwater vehicle range (m)
R_{hybrid}	hybrid glider range (m)
t	thrust deduction factor
t_{bp}	ballast pump propulsion time for upward and downward traverse (s)
t_{prop}	travel time of the glider during propeller propulsion (s)
V_A	advance velocity (m/s)
V_{bp}	horizontal velocity of the glider during buoyancy driven propulsion (m/s)
V_{prop}	horizontal velocity of the glider during propeller propulsion (m/s)
w	wake fraction
z	depth of the glider (m)
$\dot{z}$	depth rate of the glider (m/s)
α	angle of attack of the glider (deg)
Δ_{bp}	buoyancy-driven propulsion activity ratio
Δ_{prop}	propeller-driven propulsion activity ratio
η_d	propulsive efficiency (per cent)
η_{gb}	gearbox efficiency (per cent)
η_h	hull efficiency (per cent)
η_m	motor efficiency (per cent)
η_{mc}	magnetic coupling efficiency (per cent)
η_p	propeller efficiency (per cent)
η_{sys}	propulsion module system efficiency (per cent)
η_{sysm}	measured propulsion module system efficiency (per cent)
θ	pitch angle of the glider (deg)
ξ	path angle of the glider (deg)
ρ	fluid density (kg/m^3)
τ_d	delivered torque (N m)
τ_m	motor torque (N m)
τ_{sh}	shaft torque (N m)
Ω_d	delivered rotational speed (r/min)
Ω_m	motor rotational speed (r/min)
Ω_{sh}	shaft rotational speed (r/min)